CBED-MEASUREMENT OF RESIDUAL INTERNAL STRAINS IN THE NEIGHBOURHOOD OF TCP-PHASES IN NI-BASE SUPERALLOYS

Florian Pyczak, Horst Biermann, Haël Mughrabi, Andreas Volek and Robert F. Singer

Institut für Werkstoffwissenschaften, Universität Erlangen-Nürnberg,
Martensstr. 5, D-91058 Erlangen, Fed. Rep. Germany

Abstract

The influence of TCP-phases on the internal strains in the surrounding γ- and γ'-phase in two different Ni-base superalloys was investigated. One of the superalloys contained rhenium as an alloying element, while the other one did not. In the first alloy, rhenium is strongly enriched in the TCP-phases, and the phase possesses a σ- or P-type lattice structure. In the second alloy, the TCP-phase contains high amounts of the alloying elements tungsten, molybdenum and especially chromium and is of σ-type lattice structure. The method of convergent beam electron diffraction was used to determine the shear strains in the γ- and γ'-phase in an area of about one square micrometer around the TCP-phases.

Introduction and Objectives

In recent years, increasing amounts of different refractory elements were introduced in Ni-base superalloys to improve the mechanical properties. Rhenium proved to be an especially effective solid solutioning strengthener and significantly enhanced the mechanical strength of so-called second and third generation superalloys [1]. While the solid solution strengthening effects are desirable, refractory elements have also a tendency to precipitate as so-called topologically closed-packed phases (TCP-phases). It is commonly known that the presence of TCP-phases can degrade the mechanical properties of a Ni-base superalloy [2,3]. For this reason, different measures to avoid the precipitation of TCP-phases, such as careful balance of the alloy composition or homogenizing heat treatments up to 50 hours [1], are used to produce Ni-base superalloys of the second and third generation. Nevertheless, after long-term service at high temperatures, commercial alloys tend to precipitate small amounts of TCP-phases [4]. It seems that in many modern Ni-base superalloys minor contents of TCP-phases have to be accepted.

The σ-phase is the best known TCP-phase found in Ni-base superalloys until today. The lattice structure is similar to the well known σ-phase which occurs in steels, but the composition differs as tungsten, molybdenum and other alloying elements are also enriched in the σ-phase in the case of Ni-base superalloys in addition to chromium [5]. In the Ni-base superalloys of the second generation which contain rhenium, σ-phase is found and reported to contain larger contents of rhenium, but the amount of chromium is remarkably lowered. The composition is identical to another kind of TCP-phase, the P-phase which was first obtained near rhenium-containing coatings in Ni-base superalloys [6]. As mentioned above, the compositions of P- and σ-phase in Re-containing alloys are identical, but, in contrast to the tetragonal lattice cell of the σ-phase, the lattice cell of P-phase is orthogonal. The space groups and lattice parameters for the two phases are shown in Table I, and due to their structure and lattice parameters, parts of P-phase type lattice cell can be found together with parts of σ-type lattice cell in the same TCP-phase. The so-called μ-phase is the last type of TCP-phase which is frequently observed in Ni-base superalloys. The lattice structure data for μ-phase are also given in Table I. Additionally, many other types of TCP-phases, like δ-, β- or H-phase, are reported to occur in ternary systems with compositions similar

Superalloys 2000
Edited by T.M. Pollock, R.D. Kissinger, R.R. Bowman,
K.A. Green, M. McLean, S. Olson, and J.J. Schirra
TMS (The Minerals, Metals & Materials Society), 2000

Table I: Crystal structure information on σ-, μ- and P-phase [5].

TCP-phase	Space Group	Lattice Parameter (nm)
σ-phase	$P4_2/mnm$	a=0.930, c=0.486
P-phase	Pnma	a=1.720, b=0.486, c=0.920
μ-phase	$R\bar{3}m$	a=0.900, α=30.8°

to the Ni-base superalloy γ-phase [7], but none of these has been reported in the common Ni-base superalloys.

The purpose of the present work is the investigation of the effects of TCP-phases on the strains in the surrounding γ-matrix and in the coherently embedded γ'-particles. Interactions between γ–matrix and γ'-particles through the internal coherency stresses due to the γ/γ'-lattice mismatch have been thoroughly investigated during recent years and remain an important topic of present investigations in the field of Ni-base superalloys [8,9,10]. In this regard, the method of convergent beam electron diffraction (CBED) as a tool to measure lattice parameters and lattice misfits with high precision and an extremely high lateral resolution, is widely applied in Ni-base superalloys [11,12,13,14,15,16]. Kaufman et al. extended the usage of CBED to the investigation of strains induced by α-Mo precipitates in surrounding γ'-particles in a ternary Ni-Al-Mo alloy [17]. In the present work, CBED was used to characterize lattice distortions in both the γ- and the γ'-phase in the vicinity of TCP-phases. These lattice distortions induced by the TCP-phases are localized in areas of about 1 square micrometer. Thus, CBED is the ideal method to investigate these strain fields.

Experimental

Specimens

Two experimental directionally solidified Ni-base superalloys were investigated. Both are developed for the use as turbine blade material in stationary gas turbines, and their composition is based on that of the commercial alloy IN792. One alloy, later referred to as alloy A, contains up to 3wt.% of the element rhenium, and the second, subsequently referred to as alloy B, contains no rhenium. To enhance the properties of these experimental alloys compared to IN792, the contents of the elements Mo, W, Ti and Ta were also increased by 1 to 2 wt.%.

The specimens investigated in this work were aged for 500 h at 1000°C in air. Under these conditions, TCP-phases precipitate in both alloys and can be clearly recognized in the scanning electron microscope pictures (SEM), as shown in Figure 1. The shape of the precipitates is needle- or plate-like with an orientation of 45° relative to the γ'-cubes in a {001}-section. This results from certain lattice orientation relationships which are found between the different types of TCP-phases and the surrounding γ- and γ'-phase, as reported by several authors [5,18]. TEM-specimens of both alloys were produced from sections perpendicular to the solidification direction (lying close to [001]) by mechanical grinding and subsequent electrochemical polishing in an electrolyte of perchloric acid and acetic acid. By the use of chemical polishing, it is possible to avoid the introduction of strains during specimen preparation which is sometimes the case, if specimens are produced by ion milling.

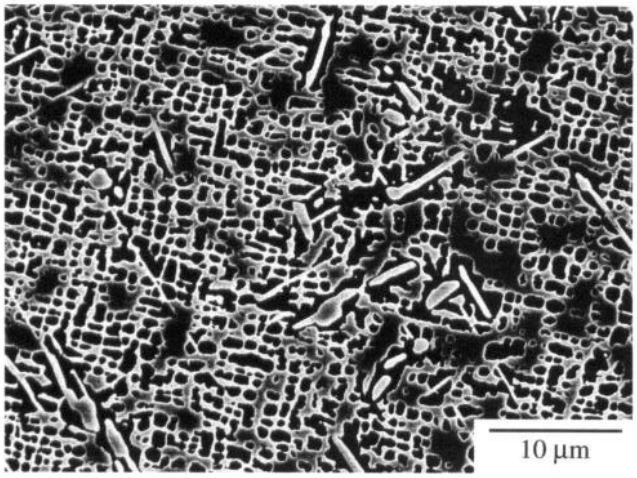

Figure 1: TCP-phases in alloy B in a scanning electron microscope image of a {001}-section.

Experimental set-up

All TEM-measurements were performed on a Philips CM200 TEM at an acceleration voltage of 120 kV or 200 kV, respectively. For CBED-measurements, a Gatan cooling stage was used, and the specimens were cooled to the temperature of liquid nitrogen to enhance the contrast in the CBED-patterns. All CBED-measurements were performed at an acceleration voltage of 120 kV. Spot sizes between 7 and 9, which result in nominal beam focuses between 27 and 15 nm, were utilized. In γ'-particles, in which relatively homogenous strain states were encountered, broader spots resulting in a higher intensity, were used, while the small focus sizes were necessary for the measurements in narrow γ–matrix channels or in the direct vicinity of TCP-phases. An incident beam parallel to the [001]-direction was chosen, because only <001>-orientations or orientations very near to <001> allow measurements in the very narrow γ-matrix channels. Furthermore, tetragonal lattice distortions are clearly distinguishable from shear distortions in <001> zone axis CBED-patterns.

All other TEM-investigations, including energy dispersive spectrometry (EDS) and the recording of selected area diffraction patterns (SAD-patterns) for the different phases, were performed using an acceleration voltage of 200 kV. The contamination of the specimens, while performing the EDS-measurements, was reduced by use of the Gatan-cooling stage. The EDS-measurements were done in the scanning mode of the TEM, working with a nominal spot diameter of about 4 nm.

Evaluation of CBED-patterns

The experimental patterns were compared with simulated patterns, calculated by using the kinematic routines of the EMS-simulation package by Stadelmann [19]. A set of patterns for pure shear distortions in a range of 0.15° were calculated for comparison with the experimental patterns. From the analysis of these simulated patterns we found that the length ratio between the two orthogonal axes parallel to the <110>-directions in the <001> zone axis CBED-pattern, which will be later referred to as R-ratio (see Figure 2), is very sensitive to changes in the angle γ of the lattice cell,

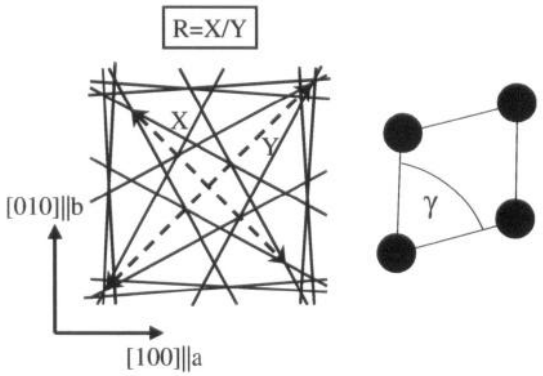

Figure 2: Simulated CBED-pattern of a shear-distorted lattice cell and a sketch of the lattice cell. The axes used to calculate the R-ratio are marked.

but is in no way recognizably influenced by pure tetragonal distortions of the lattice cell. This was also checked by kinematic simulations of CBED-patterns. In the following, a coordinate system with the lattice parameter c parallel to the [001]-direction is used. Hence, γ is the angle in the plane of the (001)-oriented specimens between the lattice axes a and b as drawn in Figure 3. It is obvious that, if the TCP-phase induces a compressive strain along the $[1\bar{1}0]$-direction, a shear component, which decreases the angle γ in the way shown in Figure 3 always exists. These shear components of the induced strain have been investigated in this work and later are simply termed as shear strains.

The CBED-patterns can be oriented due to the magnetic rotation of the TEM. Hence, directions in reciprocal space and the appropriate direction in image space can be identified as shown in Figure 4. The R-ratios of the experimental CBED-patterns were measured by using an image analysis program. By comparing the measured

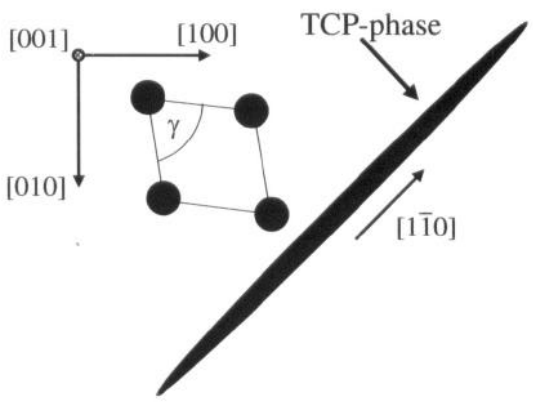

Figure 3: Schematic diagram of the used coordinate system. The lattice cells in both alloys are always under compressive strain along that <110> direction which is parallel to the long axis of the TCP-phase, as shown in the figure.

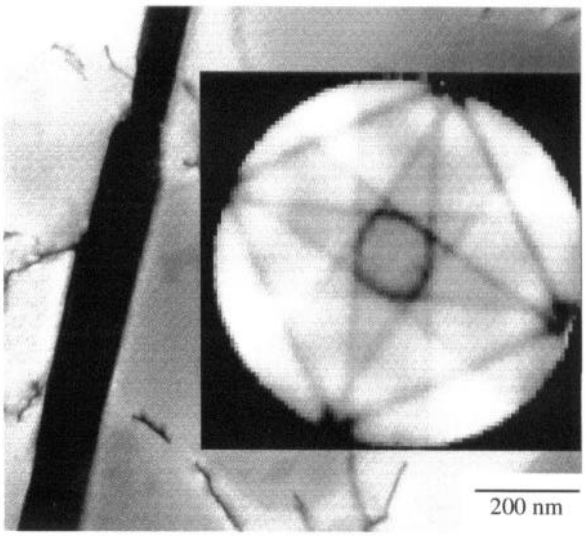

Figure 4: TEM-image of a TCP-phase together with an appropriately oriented <001> zone axis CBED-pattern.

R-ratios with a calibration curve derived from the simulated patterns, it was possible to determine the angle γ of the lattice cell [20] with an accurracy of better than 0.01°. Due to the 45°-inclination of the TCP-phases with respect to the edges of the γ'-cubes, their presence should induce a recognizable shear distortion in the <001> zone axis CBED-patterns, in their direct vicinity. As mentioned above, these shear distortions are distinguishable from tetragonal distortions, which could also be caused by the lattice misfit between γ- and γ'-phases [8,10,14]. This is shown in Figure 5, by examples of CBED-patterns of a tetragonally distorted and a tertagonally and, additionally, shear-distorted lattice cell.

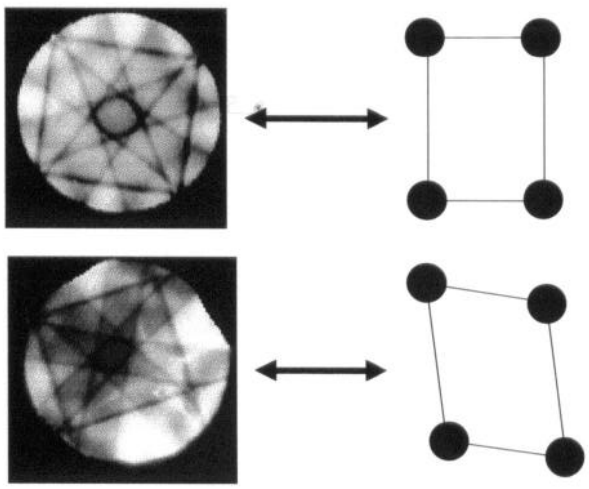

Figure 5: Schematics of a tetragonally distorted lattice cell together with the appropriate {001}-CBED-pattern and the same for a tetragonally and, additionally, shear-distorted lattice cell

Results

Microstructural investigations and SAD-measurements

The TCP-phases have been investigated by scanning electron microscope (SEM) and conventional TEM-imaging. As mentioned above, the TCP-phases in both alloys appear in SEM-images as needle-shaped particles, which are always oriented at an angle of 45° relative to the edges of the γ'-cubes. For alloy A, the concentration of TCP-phases in dendritic cores seems to be higher than in interdendritic regions (see Figure 6), in correspondence with the well-known tendency of rhenium to segregate in the dendritic cores [21]. In both alloys, the widths of the TCP-phases vary between 0.2 and 0.5 µm. Their lengths range from 10 to 20 µm in the case of alloy A and up to 100 µm in the case of alloy B.

No further microstructural features of the TCP-phases such as for example, faulting were detectable in the TEM brightfield-pictures in addition to the results obtained already in the SEM.

SAD-patterns of the TCP-phases in both alloys were taken to identify the type of investigated TCP-phase. In both cases, the TCP-phases were oriented in such a way that diffraction patterns of high symmetry were obtainable. The orientations in both cases were between the <112>- and <113>-orientations of the γ/γ'-phase, which was determined with the help of Kikuchi patterns, as shown in Figure 7 and Figure 8. From the diffraction patterns, the TCP-phase in alloy B (see Figure 7) was identified as σ-phase. The calculated lattice parameters of 0.884 nm for the a and b directions is in fair agreement with the lattice data known from literature [5,7,22,23].

For the TCP-phase in alloy A, the identification is not so unambiguous. Appropriate indexing of the diffraction patterns was possible for a P-type lattice cell as well as for a σ-phase type lattice cell (see Figure 8). Kikuchi patterns of the TCP-phase supplied no further information, since due to the thickness of the phase no clearly visible Kikuchi bands were observable.

EDS-measurements

The TCP-phases in both alloys consist mainly of elements which are enriched either in the γ-matrix, such as chromium or evenly distributed between the γ/γ'-phases, such as tungsten. Elements

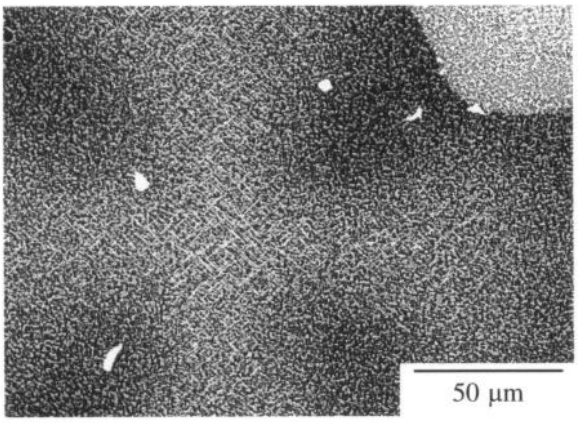

Figure 6: The SEM-picture shows clearly the higher concentration of TCP-phases in the dendritic cores in a (001) section of alloy A.

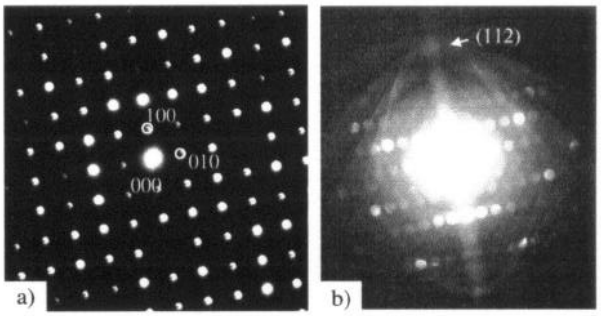

Figure 7: SAD-pattern of the TCP-phase (a) and the Kikuchi pattern of the same orientation for the neighbouring γ/γ'-phases (b) for alloy B.

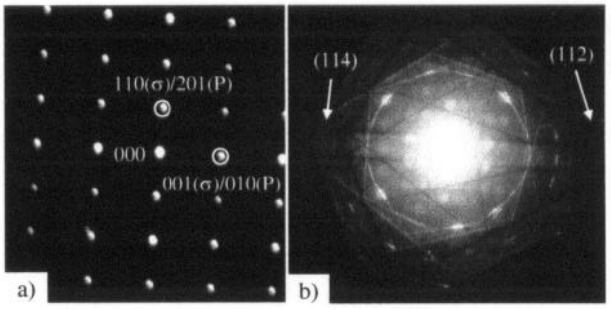

Figure 8: SAD-pattern of the TCP-phase with an indexing for σ- and P-type lattice cell marked (a). Kikuchi pattern for the neighbouring γ/γ'-phases in alloy A (b).

known as γ' builders, like titanium or tantalum, are not encountered in significant amounts in the TCP-phases. The exact compositions for both TCP-phases are shown in Table II. The refractory elements tungsten and rhenium in alloy A and tungsten in alloy B especially tend to be enriched in the TCP-phases, while the level of nickel is reduced relative to the surrounding matrix. In the TCP-phases of alloy A, high amounts of rhenium and tungsten are concentrated, while the level of chromium corresponds to that found in the matrix phase. The level of molybdenum is also enhanced compared to the γ-matrix composition.

In the TCP-phases in alloy B, mainly chromium and a remarkable amount of tungsten and molybdenum were found. However, the tungsten content in the TCP-phases of alloy B is not as high as in alloy A. No γ'-builders like tantalum or titanium were found in the TCP-phases.

Table II: Composition of the TCP-phases in the two different alloys in wt.% (elements which only occur in contents below 1% are omitted).

	Cr	Co	Ni	W	Mo	Re
Alloy A	18.8	5.0	10.0	29.1	8.4	26.6
Alloy B	32.4	11.8	23.0	20.3	12.6	0

CBED-measurements

In the present work, shear-distortions are only found near TCP-phases. They are clearly identified in the CBED patterns and are easy to distinguish from pure tetragonal distortions. The latter are recognizeable without difficulty in CBED-patterns of <001>-zone axes by examining the length inequality between the two principal axes parallel to <001>-directions [10].

In both alloys, the lattice spacings oriented parallel to the TCP-phases are compressed. This can be verified by aligning the CBED-patterns according to the magnetic rotation of the TEM. Then, the directions in the diffraction patterns correspond directly to directions in the images (see Figure 4).

It is very difficult to deduce direct connections between the induced shear strain and the distance from the TCP-phase. Obviously, in both alloys, shear distortions far above the level encountered elsewhere are measured in the direct vicinity of TCP-phases. These shear distortions vanish at larger distances from the TCP-phase which normally lie in the range of 400 to 800 nm in alloy A and 800 to 1000 nm in alloy B. However, the exact dependence of the shear distortions on the distance from the TCP-phase seems to be strongly modified by the presence of microstructural features such as dislocations or the shape of γ'-particles and matrix channels. Taking this into account, it is necessary to observe the microstructure near all individual sites of measurement, in order to understand the effects on the measured shear strains.

In alloy A, the strong shear distortions in the γ'-particles in the direct vicinity of the TCP-phases result in angles γ of about 89.95° which are encountered at distances between 70 to 300 nm away from the TCP-phases. At distances above 600 nm, the angles γ differ between 89.99° and 90.00° for all series of measurements. This corresponds to negligible shear distortions, since the shear strains measured in areas of the alloy far away from TCP-phases are in the same order of magnitude. In the γ-matrix, the tendency is similar to the situation in γ'-particles. Up to 400 nm away from the TCP-phase, shear distortions are clearly recognizable. At a distance of 600 nm from the TCP-phase, the shear distortions in the γ-matrix also vanish totally.

Two examples of series of measurements for alloy A are discussed in the following. In the first case (see Figure 9 and Figure 10), measurements in a γ'-particle directly connected to the TCP-phase and in a neighbouring matrix channel were performed. The slightly rafted γ'-particle is oriented at 45° relative to the TCP-phase. This is the situation normally found in the alloy due to the orientation relationships between TCP-phases and γ'-particles, as mentioned above. The relationship between shear strain and distance from the TCP-phase is very similar in the γ'-particle and the matrix, but the range of induced shear strains in the matrix seems to be greater. In both cases, the strong shear distortions remain, up to distances of ca. 300 nm. At larger distances, the shear distortions decrease rather abruptly and become similar to those encountered in other regions of the specimen, where no TCP-phases are present.

The series of measurements in an irregulary shaped γ'-particle shown in Figure 11 reveals another picture. Though the maximum shear distortion in the immediate vicinity of the TCP-phase is similar to the case presented above, the decrease of shear strain with increasing distance from the TCP-phase occurs smoothly and not as abruptly, as in the previous example, until an undistorted strain state is found at about 800 nm distance from the TCP-phase (see Figure 12).

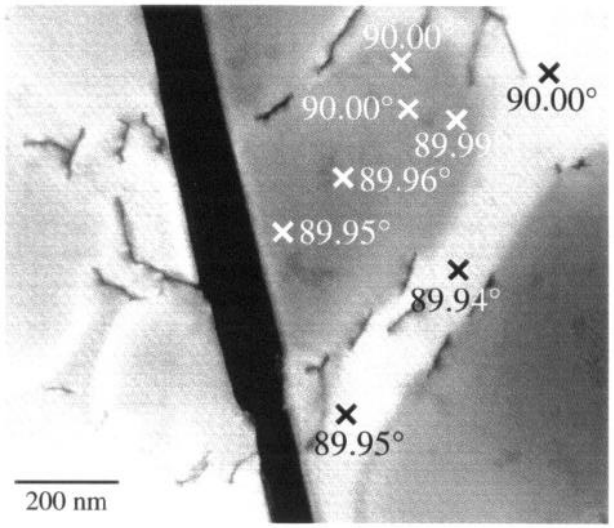

Figure 9: A series of CBED-measurements in alloy A: The measurement positions and the measured angles γ are marked.

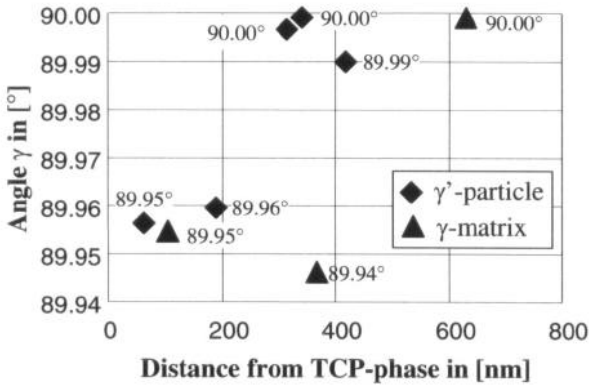

Figure 10: Angle γ plotted versus distance from TCP-phase for the series of measurements in γ- and γ'-phase in Alloy A shown in Figure 9. Triangles mark measurements in γ-matrix and squares measurements in γ'-particles.

In alloy B, the sphere of influence of the TCP-phases on the shear strains extends to much larger ranges. Measurements in γ'-particles directly connected with the TCP-phase result in angles γ between 89.84° and 89.92°. It is remarkable that, even in γ'-particles which are not directly connected to the TCP-phase but separated by one γ-matrix channel, shear distortions of the lattice cell of the same level as in direct vicinity to the TCP-phase in alloy A are encountered.

As in the case of alloy A, we shall now discuss several measurements in alloy B in more detail. As a first example, we take a series of measurements in the γ'-phase in a precipitate directly connected to the TCP-phase and a precipitate separated by one γ-matrix chan-

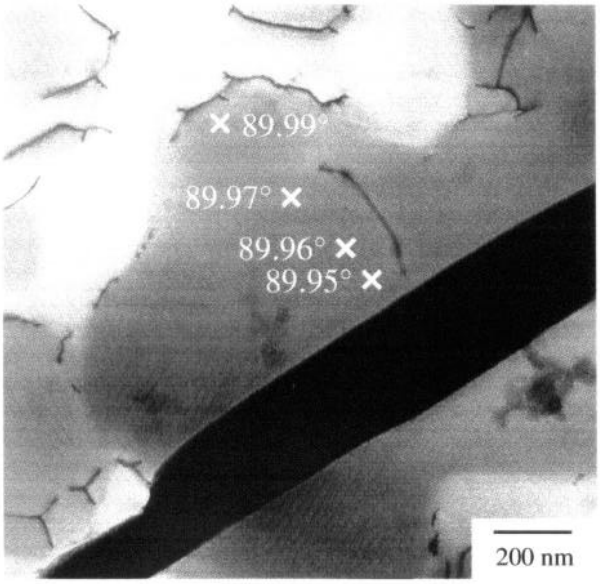

Figure 11: Series of CBED-measurements in a γ'-particle in alloy A. The beam positions and the measured angles γ are marked in the image.

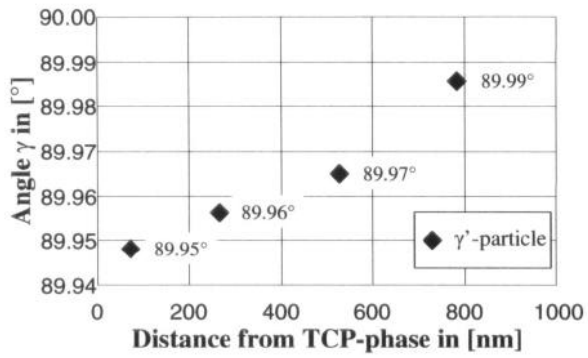

Figure 12: Angle γ plotted versus distance from TCP-phase for a series of measurements in the γ'-phase in alloy A shown in Figure 11. Compared with the results shown in Figure 10, the shear distortions have a greater lateral range and a smoother decay over the distance.

nel (Figure 13). The microstructure near the TCP-phase is very inhomogeneous in this measurement, because of some dislocations in the γ'-particle which is directly connected to the TCP-phase, and a γ-matrix channel penetrating partially into that γ'-particle. Regarding the measured shear distortions plotted in Figure 14, it is quite obvious, that stronger shear distortions occur in the areas of the γ'-particle, where no dislocations are present, compared to the level of shear distortions measured in areas, where dislocations are present. Even in the γ'-particle, which is separated by a matrix channel from the TCP-phase, shear strains are measurable at a position more than one micrometer away from the TCP-phase. It is unlikely that these shear distortions are caused by lattice mismatch between γ- and γ'-phase, because the position is in the centre of the γ'-particle, where strain states due to γ/γ'-lattice mismatch should be of hydrostatic nature.

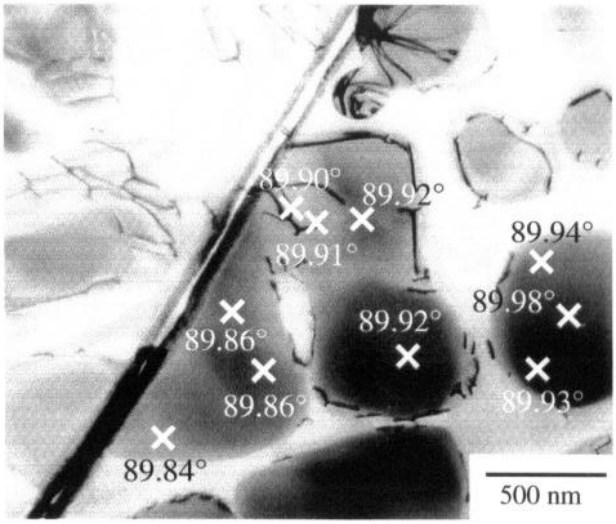

Figure 13: CBED-measurements in alloy B in a γ'-particle directly connected with the TCP-phase and a γ'-particle separated from the TCP-phase by one γ-matrix channel. Even at the measurement positions in the separated γ'-particle a shear distortion is recognizable.

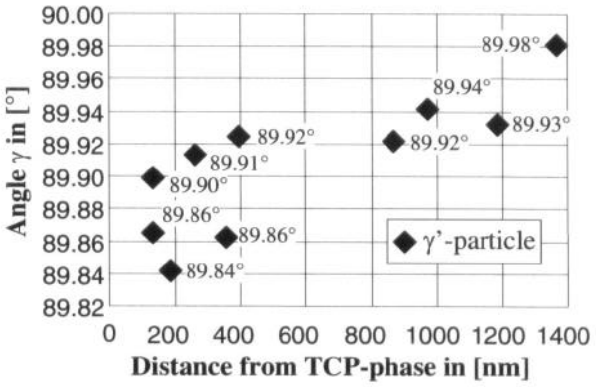

Figure 14: Angle γ plotted versus distance from TCP-phase for the series of measurements in Alloy B shown in Figure 13.

In a second example, measurements in the γ- and the γ'-phases near two closely neighbouring TCP-phases are shown (Figure 15). The respective changes of angle γ are shown in Figure 16. In the matrix phase, shear distortions near the TCP-phase are more intense than in alloy A, reaching an angle γ of 89.91° at a distance of about 200 nm from the TCP-phase. Also at a distance of 600 nm, the shear strains are much more intense than in alloy A. The picture in the γ'-phase is surprising at first sight, as slight shear distortions, leading to an angle γ of 89.97°, are encountered in a measurement position which is only 600 nm away from the TCP-phase. At this distance, shear distortions of a much higher level were measured in the series presented above (see Figure 13). But, when the microstructure of these two measurement series are compared, it is obvious that in the latter case, there is always a γ-matrix area between the measurement position and the TCP-phase, which could be responsible for the decrease of the shear strains.

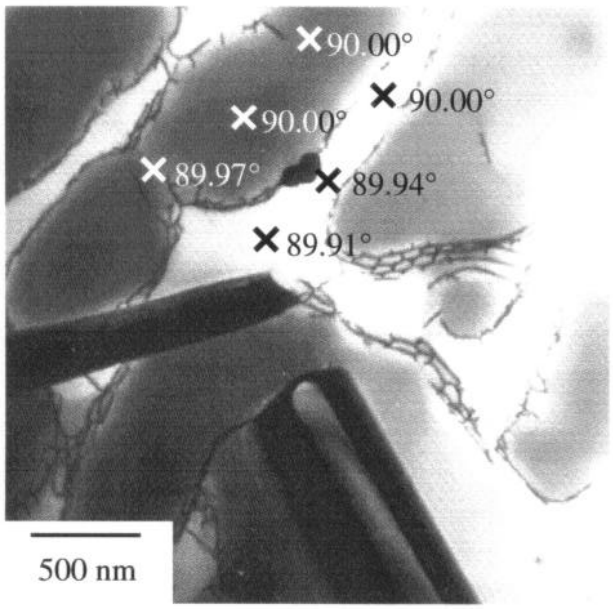

Figure 15: Two series of CBED-measurements in alloy B, one in a γ'-particle and the other in a γ-matrix channel. For all three positions in the γ'-particle the direct junction to the TCP-phase is separated by a γ-matrix channel.

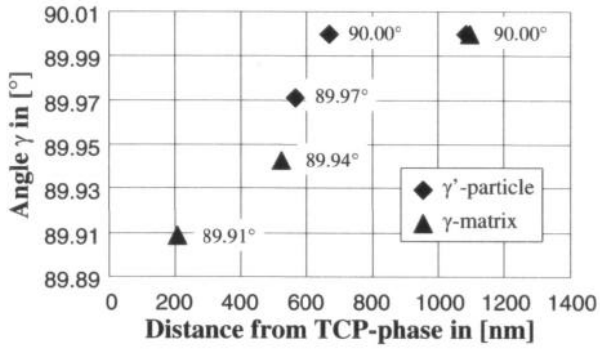

Figure 16: Angle γ plotted versus distance from TCP-phase for the measurement in alloy B shown in Figure 15. Triangles mark measurements in γ-matrix and diamonds measurements in γ'-phase.

Discussion

Type of the TCP-phase

The presented identification of the TCP-phase occurring in alloy B as a σ-phase is considered to be relatively reliable, although no useful diffraction patterns of other high symmetry orientations were obtainable from the (001)-oriented specimens used in this work, to cross-check the orientation determination. The lattice parameters obtained are in good agreement with literature data [5,7,22,23], especially if one takes into account, that the lattice parameters normally are influenced by the composition of the non-stoichiometric TCP-phases. The occurrence of σ-phase is not unexpected as σ-phase is commonly found in Ni-base superalloys which contain no rhenium and have an alloy composition which promotes the precipitation of TCP-phases. The chemical composition of the phase also supports the identification as σ-type as discussed in the next section.

The identification of the TCP-phase in alloy A is ambiguous, because an identification as σ-phase as well as P-phase is reasonable, based on the diffraction patterns. It can be excluded that the investigated TCP-phase possesses a μ-type lattice structure, because the experimentally recorded diffraction pattern and a diffraction pattern of μ-type lattice structure in any possible orientation show no correspondence.

It is presently unclear how strongly the uncertainties regarding a full identification of the investigated TCP-phases, impair the appreciation of the results, concerning the induced strains due to the presence of TCP-phases. Even for the same type of lattice structure, the lattice parameters for TCP-phases, which can be found in the literature [5,7,22,23,24], vary in a remarkable range. Also very little is known about the properties of the interface between the γ/γ'-phase and the different TCP-phases. All these questions have to be answered first, before it can be judged, whether for example the lattice structure or the chemical compositions and their influence on the lattice parameters are the most important effects which affect the strains in γ/γ'-phase.

Composition of the TCP-phases

The compositions measured by EDS correspond well with data known from the literature. Dariola et al. also report [5] that the chromium content is greatly enhanced in σ-phases which contain no rhenium. This is also true for the σ-phase in alloy B. The chromium contents of TCP-phases in rhenium-containing alloys, for σ-phase as well as P-phase, is reported to be lower and similar to the chromium-content in γ-phase [5]. This was also found for the TCP-phases in alloy A.

The refractory elements rhenium and tungsten are strongly enriched in the TCP-phases in alloy A, and their combined amount reaches more than 50 % which is three times more than in the γ-phase. Compared with the amount of tungsten in the TCP-phases in alloy B, which exceeds the tungsten content in the γ-phase at most by a factor of two, the prominence of the refractory elements in the TCP-phases of alloy A is obvious. Rhenium and tungsten levels of the same magnitude are also reported in the work of Dariola et al. [5].

Unfortunately, the measured TCP-phase compositions give no hint on the type of TCP-phase, which is encountered in alloy A, because the compositions of rhenium-containing σ-phase are reported to be identical with that of P-phase and sometimes both phases are found together in the same alloy. The phase composition in alloy B corresponds well with the data known from literature for σ-phase in rhenium-free alloys and thus confirms the results obtained by phase-identification via SAD-diffraction.

Shear strains induced in γ- and γ'-phase

It is obvious that, due to the presence of TCP-phases, shear strains in an area of about one square micrometer are induced in the surrounding γ-matrix and γ'-particles. This can be seen in Figure 17, where all measured shear distortions for both alloys are plotted

versus the distance from the TCP-phase. It is obvious, that the shear distortions obtained in alloy B are for the most cases higher than in alloy A. Some deviations can be explained by the influence of microstructural features near the measurement positions (see Figure 15 and Figure 16) and are discussed in detail below. The difference between shear strains in the matrix phase and in the γ'-particles is not significant in both alloys. Especially at measurement positions in direct vicinity of the TCP-phase, the induced shear strains in matrix phase and γ'-phase are of the same magnitude.

The magnitudes of the measured shear strains appear reasonable, if one considers the stresses associated with strains of similar magnitude. Assuming a shear modulus of the γ'-phase of 120 GPa, then shear stresses of 90 MPa in alloy A and 350 MPa in alloy B are found for the maximum shear strains measured in both specimens. These values are below the flow stress of both alloys at the temperature of measurement.

The different series of measurements presented above suggest that the correlation between the induced shear strains and the distance between TCP-phase and measurement position is not unique. The shear distortions are obviously partially influenced by locally present microstructural features, such as dislocations or γ'-particles of different shapes. The measured shear strains in the γ'-particle in Figure 15 are almost negligible and lower than in the γ-phase, suggesting that the specific distortion energy is lower than in the γ'-phase. The presence of dislocations also seems to decrease the intensity of induced shear strains, but no regular dislocation arrangements, comparable to the kind developing at γ/γ'-interfaces [26], are observed to compensate the lattice mismatch. The data available at present is insufficient to conclude whether dislocations really reduce the induced shear strains in a systematic manner.

It is commonly known that TCP-phases are not the only source of internal strains in Ni-base superalloys. The strains due to lattice mismatch between γ- and γ'-phase have been investigated thoroughly in the past [8,9,10,11,12,13,14,15,16,17]. In order to measure solely the effects of the TCP-phases, one has to find a method to separate strains induced by γ/γ'-mismatch from the strains induced by the TCP-phase. The observation, that intense shear distortions are encountered near TCP-phases, is helpful in this regard, because it is reasonable and confirmed by measurements, that the γ/γ'-mismatch induces mainly tetragonal distortions. Only near γ/γ'-interfaces, at corners of γ'-particles and in narrow matrix channels some shear distortions are present [10]. However, in the two alloys investigated, these shear distortions are far below the levels observed in the vicinity of TCP-phases. Hence, one can assume that shear distortions above a certain level are caused mainly by the presence of TCP-phases. Nonetheless, we suppose that TCP-phases also induce tetragonal distortions in the surrounding γ- and γ'-phase which can, however, not be distinguished from the effects due to the γ/γ'-mismatch.

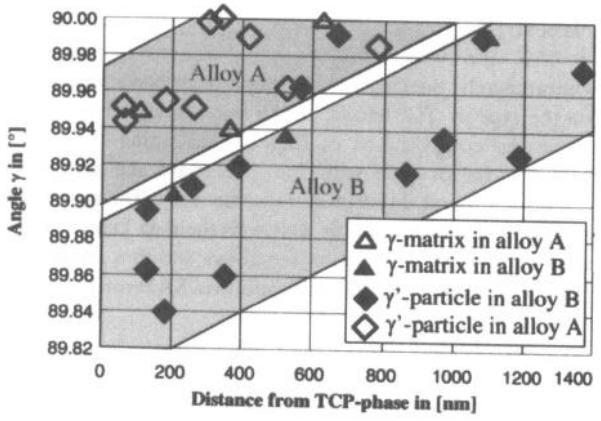

Figure 17: All measured shear strains in both alloys plotted versus distance from the TCP-phase.

On the one hand, CBED is the only method known to the authors that is able to measure such localized strain states [25]. On the other hand, the value of the information obtained is uncertain with respect to any conclusions regarding the properties of a bulk material at service temperature. The strain and stress states in a thin TEM-specimen are not equivalent to the situation in the bulk material. Hence, it is difficult to infer reliably from information obtained from thin specimens the strain states in bulk material. Another difficulty of CBED-measurements arises from the fact that the specimen must be cooled down to the temperature of liquid nitrogen in order to obtain CBED-patterns of useful quality. As the service temperature for Ni-base superalloy applications lies normally between 600 and 1100°C, results obtained at liquid nitrogen temperature provide no direct information on the influence of certain internal strains and stresses on the properties of the material under service conditions [9]. Thus, even marked differences between the measured intensities of the induced shear strains near the TCP-phases in the two different alloys do not, at present, permit any valid conclusions as to how this would affect the mechanical properties under service conditions. At the present state of this study, it is premature to decide whether the data obtainable by CBED-measurements could provide a potentially useful basis for simulations in order to model the situation at service temperature.

Significance of TCP-phases for damage initiation

The presence of a third phase with elastic moduli and thermal expansion coefficients which deviate strongly from that of γ-matrix and γ'-particles may have strong effects on the mechanical properties and on the damage behaviour of the superalloy. The elastic hardness of the TCP-phases is assumed to be high compared with the surrounding two-phase compound. Hence, externally applied stresses cause elevated internal stresses in the TCP-phases. The fracture of the brittle TCP-phase under these circumstances could degrade the fatigue properties of the superalloy, because the broken TCP-phases could act as initiation points for cracks. The differences in thermal expansion coefficients can also affect the properties of a Ni-base superalloy in service. Temperature changes from ambient temperature to elevated service temperatures and back to ambient temperature or temperature changes during service often occur in a Ni-base superalloy turbine blade, e.g. at the start-up of a jet engine turbine. During these temperature changes, the differences in thermal expansion coefficients cause thermally induced internal strains in the TCP-phases and in the surrounding superalloy. These internal strains are either compensated by elastic deformation of the TCP-phase and the superalloy, leading to the

corresponding internal stresses, or by plastic deformation of the superalloy at the interfaces between TCP-phase and γ/γ'-compound. In this investigation, no evidence of plastic deformation of the γ/γ'-compound, i.e. a higher dislocation density near the TCP-phases compared with other regions, has been found. If thermally induced internal stresses occur due to the presence of TCP-phases, they are superimposed on the externally applied stresses and increase the superalloy's probability of failure due to the fracture of the TCP-phases. As these internal stresses are not homogeneously distributed over the whole superalloy, but concentrated near the TCP-phases, these stress concentrations will probably cause fracture of the TCP-phase or decohesion between the TCP-phase and the surrounding γ/γ'-compound.

As outlined above, it is important to be concerned about the effects of TCP-phases on the mechanical properties of a Ni-base superalloy not only at service temperature but also during temperature changes. Although the data presented allow no conclusions, whether one of the two TCP-phases affects the mechanical properties of the superalloy at service temperature more than the other by inducing internal strains in the surrounding γ/γ'-compound, it can be determined from the results, that the effects of the two TCP-phases on the mechanical properties must be different with regard to temperature changes. The effects of the TCP-phases in alloy A and B are different at the temperature of the measurement, where the strains in alloy A are significantly smaller. Even if at one temperature, and by chance this may even be the service temperature, the induced strains caused by the different TCP-phases are equal, the situation in both alloys during heating up to service temperature or cooling down after a thermal cycle must be different. Hence, the TCP-phase in the Re-containing alloy A obviously must have different effects on the mechanical properties of the Ni-base superalloy compared with the classical σ-phase in alloy B, as the strains induced by both TCP-phases are of significantly different magnitude. This result is especially relevant, as the importance of rhenium as an alloying element has strongly increased in recent years in modern Ni-base superalloy development.

Conclusions

In the present work, the distortions in the vicinity of TCP-phases of two experimental superalloys were investigated by CBED. The most important findings are the following:

1) The lattice structures of the two investigated types of TCP-phases in both alloys have been partially identified by the evaluation of SAD-patterns. Both TCP-phases are of σ- or P-type. The identification of the TCP-phase in the rhenium-free alloy B as σ-type is quite unambiguous and in good correlation with the measured chemical composition and the shape of the TCP-precipitates. The TCP-phase in alloy A could either be of σ- or P-type.

2) The compositions of the TCP-phases in both alloys were measured by the use of EDS in the TEM. In alloy A, mainly rhenium and tungsten and in Alloy B chromium and a minor content of tungsten are the main elements encountered in the TCP-phases. These compositions are very similar to data published in literature for both kinds of phases.

3) The presence of TCP-phases in a Ni-base superalloy induces recognizable shear strains in the surrounding γ- and γ'-phase. These shear distortions are distinguishable from internal strains caused by other microstructural features like γ/γ'-mismatch, because their magnitude exceeds the level of shear strains encountered in areas of the specimen, where no TCP-phases are present. The shear strains were confined to areas of about one square micrometer around the TCP-phase.

4) In the present work, CBED was applied to measure these shear strains, because CBED is the only method which permits measurements of lattice parameters with the necessary high lateral resolution. The shear strains can be separated from pure tetragonal distortions by investigating CBED-patterns of <001>-zone axes, and evaluating the length ratio of the axes parallel to the <110>-directions.

5) The measurements presented for two different Ni-base superalloys showed significant differences in the magnitude of the induced shear strains. Re-containing TCP-phases cause shear distortions of a much lower level in their direct vicinity than TCP-phases which consist mainly of the elements tungsten and chromium and are free of rhenium. It was impossible to deduce exactly, how the induced shear distortions are correlated with the distance from the TCP-phase, because of the interference of other microstructural features which obviously modified the local strain states.

6) Since the measurements were performed at about -180° C and because of the modified strain states due to the relaxation in the thin TEM-specimens, it is difficult to draw conclusions regarding the effects in bulk materials at service temperature.

7) Further work is necessary in order to substantiate whether data of the type presented can provide a reliable basis for simulations to calculate the internal strain and stress states caused by TCP-phases under service conditions.

Acknowledgments

This work was performed within the framework of a larger collaboration project which financially supported by the Bundesministerium für Bildung und Forschung (BMBF). This support is acknowledged gratefully. The authors also wish to thank their cooperation partners, especially DONCASTERS Precision Casting (DPC) in Bochum for the casting of the two investigated alloys.

Literature

1. G. L. Erickson, "The development and application of CMSX-10", Superalloys 1996, ed. R.D. Kissinger, D.J. Deye, D.L. Anton, A.D. Cetel, M.V. Nathal, T.M. Pollock and D.A. Woodford (Warrendale, PA: The Minerals, Metals &Materials Society, 1996), 35-44.

2. G. Chen, C. Yao and Z. Zhong, "The effect of σ phase on the mechanical properties in Ni-Cr-Co base wrought superalloys", Superalloys 1980, ed. J.K. Tien, S.T. Wlodek, H. Morrow, M. Gell and G.E. Maurer, (Warrendale, PA: American Socierty for Metals, 1980), 355-364

3. M. Simonetti and P. Caron, "Role and behaviour of μ phase during deformation of a nickel-based single crystal superalloy", Materials Science and Engineering A, 254 (1998), 1-12.

4. W. Schneider and H. Mughrabi, "Investigation of the creep and rupture behaviour of the single-crystal nickel-base superalloy CMSX-4 between 800° C and 1100° C", Proceedings 5th International Conference on Creep and Fracture of Engineering Materials and Structures, ed. B. Wilshire and R.W. Evans, (London: The Institute of Materials, 1993), 209-220.

5. R. Dariola, D.F. Lahrman and R.D. Fields, "Formation of topologically closed packed phases in nickel base single crystal superalloys", Superalloys 1988, ed. S. Reichmann, D.N. Duhl, G. Maurer, S. Antolovich and C. Lund (Warrendale, PA: The Metallurgical Society, 1988), 255-264.

6. W.S. Walston, J.C. Schaeffer and W.H. Murphy, "A new type of microstructural instability in superalloys - SRZ", Superalloys 1996, ed. R.D. Kissinger, D.J. Deye, D.L. Anton, A.D. Cetel, M.V. Nathal, T.M. Pollock and D.A. Woodford (Warrendale, PA: The Minerals, Metals &Materials Society, 1996), 9-18.

7. E. Gozlan et al., "Topologically close-packed precipitations and phase diagrams of Ni-Mo-Cr and Ni-Mo-Fe and of Ni-Mo-Fe with constant additions of chromium", Materials Science and Engineering A, 141 (1991), 85-95.

8. H.A. Kuhn, H. Biermann, T. Ungar and H. Mughrabi, "An X-ray study of creep-deformation induced changes of the lattice mismatch in the γ'-hardened monocrystalline nickel-base superalloy SRR 99", Acta Metallurgica et Materialia, 39 (1991), 2783-2794.

9. H. Biermann, M. Strehler and H. Mughrabi, "High-temperature measurements of lattice parameters and internal stresses of a creep-deformed monocrystalline nickel-base superalloy", Metallurgical and Materials Transactions, 27A (1996), 1003-1014.

10. B. von Grossmann, H. Biermann and H. Mughrabi, "Measurement of service-induced internal elastic strains in a single-crystal nickel-based turbine blade with convergent beam electron diffraction", Philosophical Magazine A, in press.

11. A.J. Porter et al., "Coherency strain fields: magnitude and symmetry", Journal of Microscopy, 129 (1983), 327-336.

12. D.F. Lahrman, R.D. Field, R. Darolia and H.L.Fraser, "Investigation of techniques for measuring lattice mismatch in a rhenium containing nickel base superalloy", Acta Metallurgica, 36 (1988), 1309-1320.

13. D. Mukherji and R.P. Wahi, "On the measurement of lattice mismatch between γ and γ'-phases in nickel-base superalloys by CBED technique", Scripta Materialia, 35 (1996), 117-122.

14. R.R. Keller, H.J. Maier, H. Renner and H. Mughrabi, "Local lattice parameter measurements in a creep-deformed nickel-base superalloy by convergent beam electron diffraction", Scripta Metallurgica et Materialia, 27 (1992), 1167-1172 and Scripta Metallurgica and Materialia, 28 (1993), 661 (Errata).

15. R.C. Ecob et al., "The application of convergent-beam electron diffraction to the detection of small symmetry changes accompanying phase transformations", Philosophical Magazine A, 44 (1981), 1117-1133.

16. R. Völkl, U. Glatzel and M. Feller-Kniepmeier, "Measurement of the lattice misfit in the single crystal nickel based superalloys CMSX-4, SRR99 and SC16 by convergent beam electron diffraction", Acta Materialia, 46 (1998), 4395-4404.

17. M.J. Kaufman, D.D. Pearson and H.L. Fraser, "The use of convergent-beam electron diffraction to determine local lattice distortions in nickel-base superalloys", Philosophical Magazine A, 54 (1986), 79-92.

18. M. Pessah-Simonetti, P. Donnadieu and P. Caron, "T.C.P. phase particles and prediction of the orientation relationships", Scripta Metallurgica et Materialia, 30 (1994), 1553-1558.

19. P.A. Stadelmann, "EMS - a software package for electron diffraction analysis and HREM image simulation in material science", Ultramicroscopy, 21 (1987), 131-146.

20. F. Pyczak and H. Mughrabi, "CBED-measurement of residual internal strains in the neighbourhood of TCP-phases in Ni-base superalloys", Proceedings of EUROMAT conference 1999, in press.

21. U. Brückner, A. Epishin and T. Link, "Local X-ray diffraction analysis of the structure of dendrites in single-crystal nickel-base superalloys", Acta Materialia, 45 (1997), 5223-5231.

22. J.R. Mihalisin et al., "Sigma - its occurrence, effect and control in nickel-base superalloys", Transactions of the Metallurgical Society of AIME, 242 (H) (1968), 2399-2414.

23. A. Proult et al., "Identification of the fault vectors of planar defects in the sigma phase in a nickel-based superalloy", Philosophical Magazine A, 72 (1995), 403-414.

24. J. Burslik, "The existence of P phase and Ni_2Cr superstructure in Ni-Al-Cr-Mo system", Scripta Materialia, 39 (1998), 1107-1112.

25. H.J. Maier et al., "On the unique evaluation of local lattice parameters by convergent-beam electron diffraction", Philosophical Magazine A, 74 (1996), 23-43.

26. T.P. Gabb, S.L. Draper, D.R. Hull, R.A. MacKay and M. V. Nathal, "The role of interfacial dislocation networks in high temperature creep of superalloys", Materials Science and Engineering, 118 (1989), 59-69.